Journal of Power Sources 241 (2013) 660–667

Contents lists available at SciVerse ScienceDirect

Journal of Power Sources

journal homepage: www.elsevier.com/locate/jpowsour

Rapid synthesis of porous Pd and PdNi catalysts using hydrogen bubble dynamic template and their enhanced catalytic performance for methanol electrooxidation

Ruoshi Li, Han Mao, Jingjing Zhang, Tao Huang**, Aishui Yu*

Department of Chemistry, Shanghai Key Laboratory of Molecular Catalysis and Innovative Materials, Institute of New Energy, Fudan University, Shanghai 200438, China

HIGHLIGHTS

- Porous Pd and Pd–Ni catalysts are prepared using hydrogen bubble dynamic template.
- The catalysts have 3D hierarchical pores and interconnected dendrite walls.
- The porous catalysts show good catalytic performance towards methanol oxidation.
- The enhancement can be ascribed to the porous structure and the Ni doping effect.

GRAPHICAL ABSTRACT

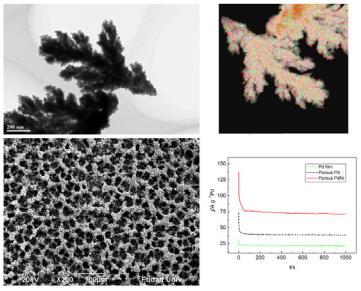

ARTICLE INFO

Article history:
Received 27 December 2012
Received in revised form
24 April 2013
Accepted 7 May 2013
Available online 17 May 2013

Keywords:
Methanol electrooxidation
Palladium–nickel catalysts
Electro-deposition
Hydrogen bubble dynamic template
Porous catalysts

ABSTRACT

Pd and Pd–Ni catalysts with three-dimensional hierarchical pores consisting of interconnected dendrite walls are successfully fabricated by cathodic deposition using hydrogen dynamic bubble template. The as-prepared catalysts are characterized by scanning electron microscopy, X-ray diffraction, transmission electron microscopy, energy dispersive X-ray spectroscopy, element analysis mapping, X-ray photoelectron spectroscopy and typical electrochemical measurements. It is found that the porous structure enlarges the electro-active surface area; the Ni doping modifies the electronic structure of the catalysts and improves their stability. Thus the porous catalysts exhibit excellent catalytic activity and stability towards methanol oxidation.

1. Introduction

Direct methanol fuel cells (DMFCs) are thought to be promising power sources for portable electronic devices because of the high energy density, simple construction, easy operation and environmental benignity [1–3]. For practical applications one of the key issues is the design of effective and low-priced anode catalysts. Among the various electrocatalysts, Pt-based catalysts were most widely studied because of their good activity towards methanol oxidation [4–6]. However, Pt is susceptible to poisoning by the reaction intermediates such as adsorbed CO. In addition, the high cost and scarcity of Pt also hindered its large-scale application. Therefore much efforts have been made to develop low Pt loading or Pt-free catalysts, among them, Pd is considered as a good alternative due to its lower cost, better resistance to CO poisoning and high activity in alkaline media for methanol oxidation [7–13]. Nevertheless, the activity and stability of pure Pd are not satisfactory and needs further improvement for commercialization.

* Corresponding author. Tel./fax: +86 21 51630320.
** Corresponding author. Tel.: +86 21 51630321; fax: +86 21 51630320.
E-mail addresses: huangt@fudan.edu.cn (T. Huang), asyu@fudan.edu.cn (A. Yu).

0378-7753/$ – see front matter © 2013 Elsevier B.V. All rights reserved.
http://dx.doi.org/10.1016/j.jpowsour.2013.05.032

On one hand, alloying with a non-precious element is a conventional way to improve the catalysts because it not only enhance the activity but also reduce the usage of precious metal. The enhancement of the catalytic properties can be achieved by bifunctional effect, synergistic effect or electronic modification by another element. In addition, alloying may also change the size and morphology of the catalysts. Several Pd-based alloy catalysts have been investigated towards methanol oxidation, such as PdSn, PdCu, PdCo, PdNi and so on [14–19]. Especially, PdNi catalysts with different morphologies have been reported to enhance the activity for methanol oxidation [20–23].

On the other hand, since electrocatalytic activity of a catalyst strongly depends on the electronic and structural properties, controllable synthetic routes of catalysts with designed microstructure are highly desirable. For example, Pd-based nanostructures including nanoflowers, nanowires, hollow spheres and nanoplates have been found to exhibit enhanced electrocatalytic activity for small molecules oxidation [24–28]. Among various nanostructured materials, porous materials are especially attractive for use as electrocatalysts because of the high electro-active surface areas (EASA). In the past two decades, great efforts have been made in controllable fabrication of porous structures. Among various synthetic strategies, template-directed synthesis and dealloying are the most popular methods. For the template-directed synthesis, hard templates such as polystyrene and silica spheres [29,30], soft templates such as lyotropic liquid crystal [31–34] and high internal phase emulsion [35,36] are commonly used to control the porous structure accurately. However, the elimination of traditional templates is complicated and may destroy the porous structure. Although the porous metals obtained by dealloying [37,38] usually have high EASA, the uniform pore size is not ideally suited for fast electrochemical reactions because the nano-pores near the top surface may restrict the transport of electro-active species (gas/ion) to the inner space of the structure, leading to low utilization of the whole surface areas because of mass transport limitations. Recently, a green and promising template, hydrogen bubble dynamic template, was proposed, by which self-supported three-dimensional porous metals such as Cu, Au, Pt, Ag et al. with highly porous dendritic walls have been successfully prepared from electrochemical deposition process [39–47]. The hierarchical structures not only allow fast mass transport of ion/gas through the electrolyte/electrode interface (due to the ordered micro-pores) but also show good activity (due to the highly porous dentritic walls). Moreover, compared to hard templates, the hydrogen bubble template possess several advantages: low cost, ease of preparation, facile control of structures, and facile one-step synthesis process, including preparation of the template, metal deposition, and elimination of the template. However, Pd–Ni porous films prepared by this route have never been reported. And the electrocatalytic properties of porous Pd and PdNi films towards methanol oxidation still need to be explored.

Combining the advantage of both porous structure and alloying, here we prepared PdNi porous films via a facile way (i.e. electrodeposition with hydrogen bubble dynamic template). To our knowledge, this is the first report about the synthesis of PdNi catalysts with three-dimensional pores consisting of interconnected dendrite walls and their electrocatalytic properties towards methanol oxidation.

2. Experimental

2.1. Preparation of Pd and PdNi porous films

Electro-deposition of the catalysts was carried out on an electrochemical workstation (CHI440A, CHI Company) using a conventional three-electrode electrochemical cell with a platinum sheet and a Hg/Hg_2SO_4, K_2SO_4 electrode (MSE) as the counter and reference electrodes at room temperature. A glassy carbon electrode (GC, Φ 5 mm) sealed by PTFE was used as working electrode for catalysts deposition. It was polished with 0.05 μm alumina powder until a shiny, mirror-like surface was obtained and then ultrasonicated for several minutes in deionized water. The GC electrode was further cleaned in 0.5 M H_2SO_4 solution by electrochemical cyclic voltammetry within the potential range from −0.75 to 0.85 V at a scan rate of 50 mV s^{-1}. Then PdNi and Pd porous films supported on GC electrodes were electrodeposited at −4 V for 60 s in a solution containing 20 mM $PdCl_2$, 0.5 M H_2SO_4 and 0.1 M NH_4Cl with or without 0.1 M $NiCl_2$. For comparison, Pd films without porous structure were electrodeposited in the same solution at −0.55 V to avoid the formation of hydrogen bubble template. The deposition time was adjusted to make sure similar amounts of Pd were obtained compared to porous Pd films. All chemicals were of analytical grade and used without further purification. Deionized water was used to prepare all solutions.

2.2. Materials characterizations

The as-prepared catalysts were characterized by X-ray diffraction (XRD), which was performed on a Bruker D8 Advance X-ray diffractometer using Cu Kα radiation with a k of 1.5406 Å. The Pd loadings and compositions of the catalysts were analyzed by means of inductively coupled plasma-atomic emission spectroscopy (ICP-AES) on a Hitachi P-4010. The morphology was observed by scanning electron microscope (SEM, Hitachi, FE-SEM S-4800A) and the composition was analyzed by an energy dispersive X-ray spectrometer (EDX) operated at 20 keV (Bruker, QUANTAX 400, attached to SEM). Transmission electron microscopy, dark-field STEM and element analysis mapping (EM) were carried out on a TEM, JEOL JEM-2010F UHR. X-ray photoelectron spectroscopy (XPS) experiments were carried out on an RBD upgraded PHI-5000C ESCA system (Perkin Elmer) with Al Kα radiation ($h\nu$ = 1486.6 eV). Binding energies were calibrated by using the containment carbon (C1s = 284.6 eV).

2.3. Electrochemical measurement

All electrochemical measurements were carried out on the same workstation using the three-electrode electrochemical cell as the electro-deposition process. The counter electrode was a Pt plate, and an MSE or a Hg/HgO electrode (MMO) was used as the reference electrode. The as-prepared catalysts were firstly characterized in 0.5 M H_2SO_4 solution at a scan rate of 50 mV s^{-1} by cyclic voltammetry and their electrochemical performance for methanol oxidation was studied by the means of cyclic voltammetry (CV), chronoamperometry (CA) and chronopotentiometry (CP). The CV measurements were carried out in 0.5 M KOH and 0.5 M CH_3OH at a scan rate of 50 mV s^{-1}. For CA test, the working electrodes were polarized at −0.1 V in the same solution for 1000 s. The CP measurements were carried out with an anodic current of 128 mA cm^{-2}.

3. Results and discussion

The morphology of the as-prepared catalysts is characterized by SEM and shown in Fig. 1. It could be seen clearly the orderly porous structure of Pd and PdNi catalysts from a1 and b1. The typical porous structure forms with the help of hydrogen bubble dynamic template: hydrogen bubbles arising from the electrochemical reduction of H^+ functioned as the dynamic template for metal electro-deposition. Metal was electrodeposited and grew within the interstitial spaces between the hydrogen bubbles and formed a

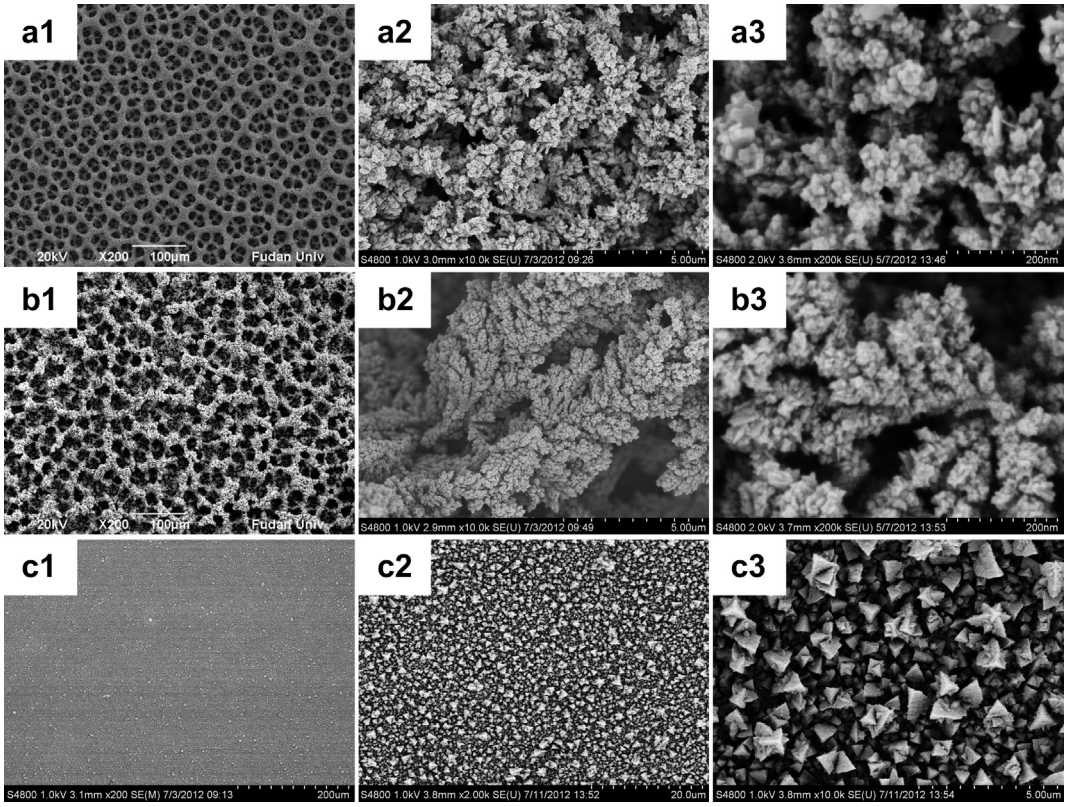

Fig. 1. SEM images of the as-prepared catalysts: (a1–a3) porous Pd film; (b1–b3) porous PdNi film; (c) non-porous Pd film.

porous film on the substrate. Compared to porous Pd, the surface of PdNi catalysts seems rougher. The morphology change of porous PdNi catalyst is probably due to the Ni alloying effect. The presence of Ni plays an import role in the nucleation and growth of PdNi alloys. It was demonstrated by C. Du et al. that the electrodeposited PdNi alloy nanoparticles had smaller size and rougher surfaces compared to Pd nanoparticles prepared under the same condition [48]. It's probably the same case for our porous PdNi alloy catalysts. In contrast, without the hydrogen bubble template, only flat films without pores were obtained, as seen in c1. Fig. 1a2 and b2 demonstrates that the wall of the pores consisted of porous dendrites. The grains of the dendrites are nanosized, revealed by a3 and b3. Compared to them, the non-porous Pd films are composed of uneven micron-sized polyhedrons which are displayed by c2 and c3. In brief, the SEM images indicate clearly the successful synthesis of porous Pd and PdNi catalysts.

Detailed information about the grain size and morphology of the dendritic walls of the porous catalysts is shown by TEM images in Fig. 2. There is not much difference between Pd and PdNi catalysts. Fig. 2a1 and b1 displays the dendritic feature of the catalysts, corresponding to SEM images. The grain size and diameter of the catalyst of dendrite branches are less than 10 nm, revealed by a2 and b2. HRTEM images in a3 and b3 demonstrate the crystallographic features. The interplanar spacing of Pd and PdNi particles or

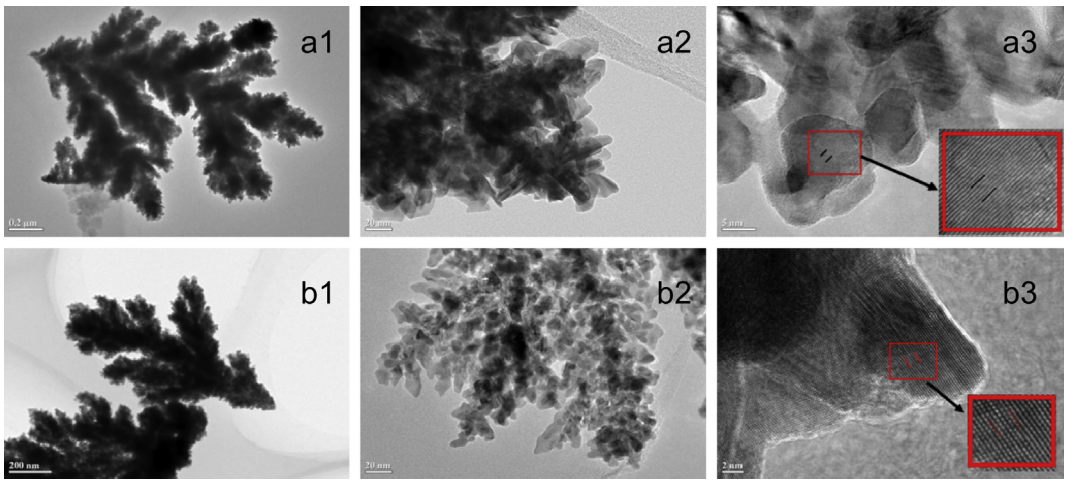

Fig. 2. TEM images of the as-prepared catalysts: (a1–a3) porous Pd film; (b1–b3) porous PdNi film.

branches is 0.223 nm and 0.208 nm, respectively, both corresponding to Pd (111) plane. The lattice contraction of PdNi catalyst can be ascribed to the formation of PdNi alloy [19].

Fig. 3 demonstrates the elemental composition and distribution of porous PdNi catalysts. EDX pattern in Fig. 3A confirms the existence of Pd and Ni element and the atomic ratio of Pd:Ni is 79:21. However, there is an inherent uncertainty in EDX data because it only shows regional composition. So the atomic percentages were further evaluated from ICP-AES and are 15.5% for Ni and 84.5% for Pd. It could be seen there is more Pd in the deposit although there is less Pd than Ni salts in the solution. It's because that the standard reduction potentials of Pd^{2+}/Pd and Ni^{2+}/Ni are quite different. It's 0.915 V for Pd^{2+}/Pd and −0.257 V for Ni^{2+}/Ni, which means it's far easier for Pd^{2+} to be reduced than Ni^{2+}. Fig. 3B shows the STEM image and the corresponding elemental mapping. It indicates that Pd and Ni distribute uniformly in the catalyst, without phase segregation. It coincides with the above conclusion of the formation of alloy (solid solution) between Pd and Ni from HRTEM results.

Fig. 4A displays the XRD patterns of the as-prepared catalysts. The peaks located at 25° and 43° correspond to the hexagonal graphite (002) and (101) plane of GC substrate (JCPDS, Card No. 75-1621). The other principal peaks exhibit the characteristics of a single face-centered-cubic (fcc) crystallographic structure of Pd (JCPDS, Card No.46-1043), corresponding to the planes (111), (200), (220), (311) and (222) located at 40, 47, 68, 82° and 87°, respectively. It also could be seen the diffraction peak of GC located in the same angle of all the catalysts, by contrast, the characteristic peaks of Pd in porous PdNi catalysts are shifted to higher 2θ values with respect to the corresponding peaks in the Pd catalysts, indicating the formation of alloy between Pd and Ni, and a contraction in the Pd–Pd interatomic distance [19]. This result corroborates the

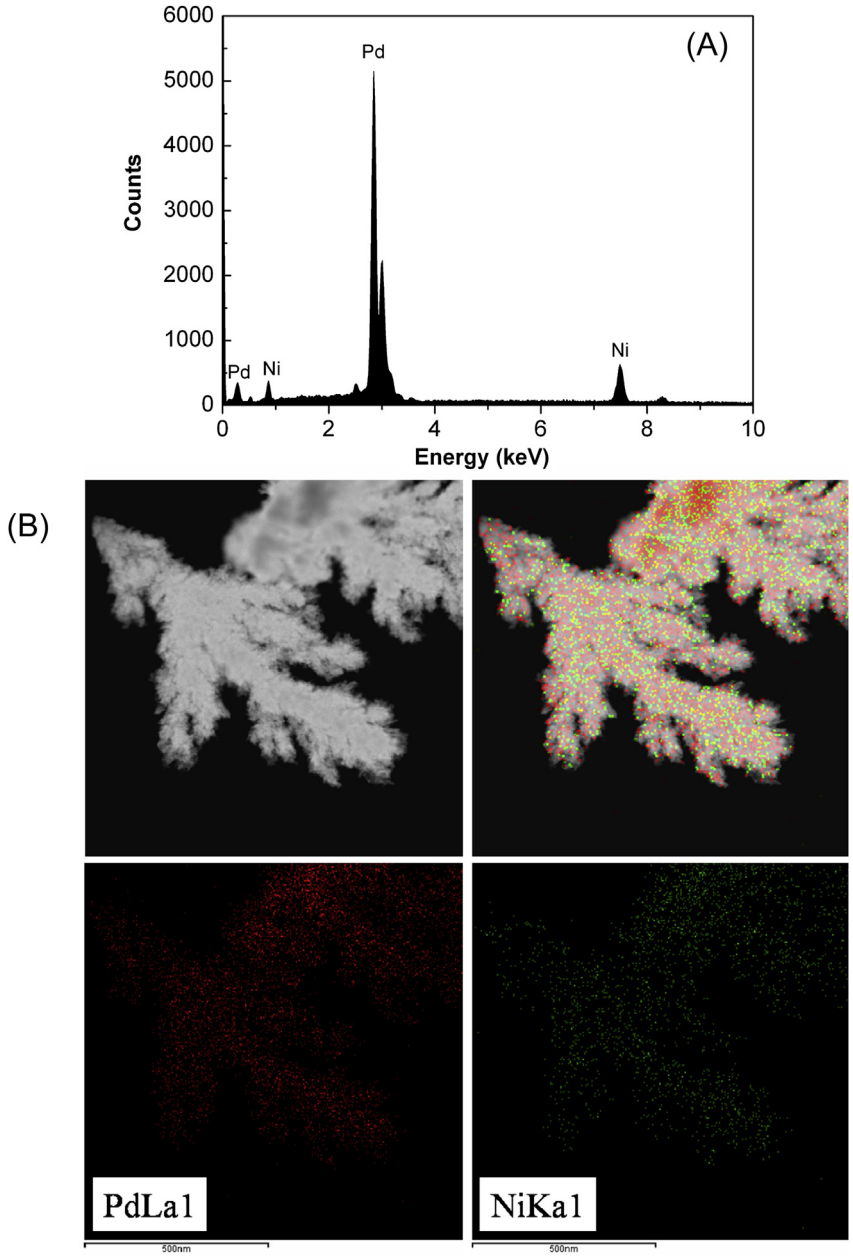

Fig. 3. (A) EDX pattern of porous PdNi catalysts; (B) dark-field STEM and the corresponding element analysis mapping of Pd/Ni.

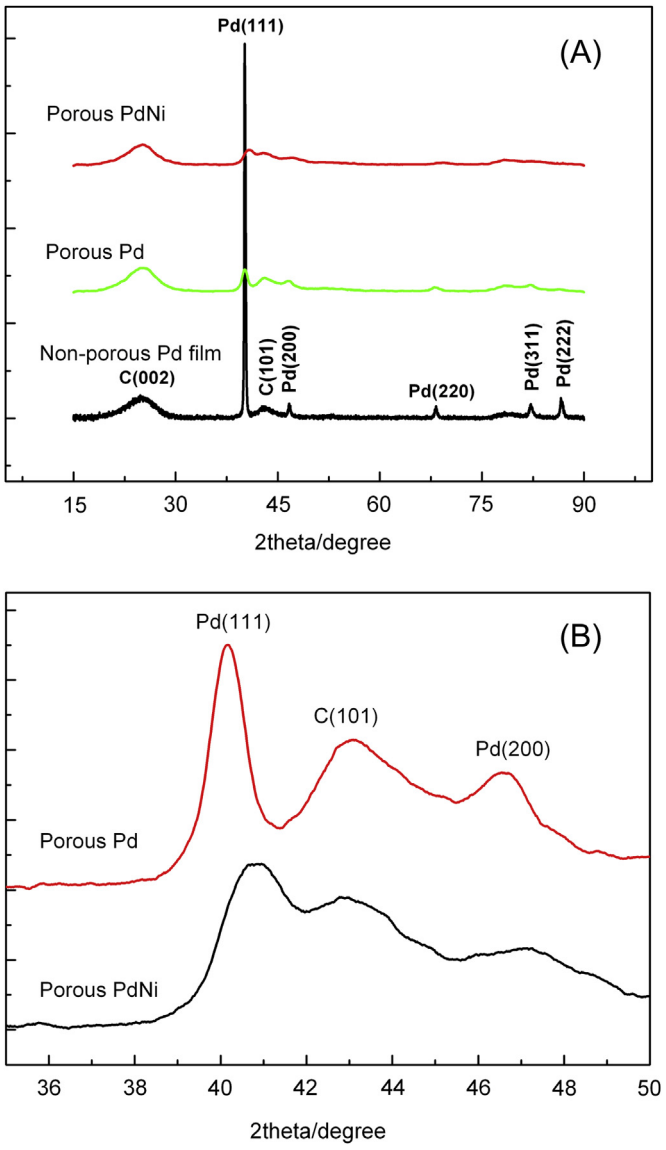

Fig. 4. (A) XRD patterns of the as-prepared catalysts; (B) sectional XRD patterns of the porous catalysts.

conclusion form HRTEM and EM described above. The shift of Pd peaks can be used to calculate the degree of alloying. The Pd (111) diffraction peak was used to analyze the lattice constant and the atomic fraction of Ni in the alloy (χ_{Ni}) of PdNi porous catalysts according to Vegard's law [49] and an empirical equation [50]. The calculated χ_{Ni} is 13.9 at.%, which is very close to the ICP-AES results (15.5 at.% for Ni), indicating that almost all Ni atoms enter into the Pd lattice to form Pd–Ni alloy. In addition, according to the Debye–Scherrer formula, particle size is inversely proportional to the FWHM of the diffraction peak. Apparently, the Pd peaks of non-porous Pd film are much sharper than others, which imply larger particle size, in accordance with the micron-size shown by SEM images. To the contrary, the Pd peaks of porous catalysts are much broader, indicating smaller particle size, proved by SEM and TEM images. Peak shift is clearer in the sectional XRD pattern in Fig. 4B. Moreover, the peaks of PdNi catalysts are a little broader than the porous Pd catalysts, indicating smaller elementary grains, which cannot be clearly shown in SEM and TEM images because of the interconnected dendritic structure.

To understand the electronic effects of Ni alloying, XPS measurements were performed to determine the chemical states of the catalyst surfaces. The XPS spectra for Pd 3d core level regions in the as-prepared catalysts are shown in Fig. 5. In order to quantify the possible oxidation states of Pd element, Pd 3d doublet splitting spectra have been fitted using a mixed Gaussian–Lorentzian function. The binding energy (BE) separation between Pd $3d_{5/2}$ and Pd $3d_{3/2}$ lines was fixed to 5.25 eV according to empirical determinations. The reported BE is associated with the Pd $3d_{5/2}$ line. De-convolution of the Pd 3d signal was achieved using three

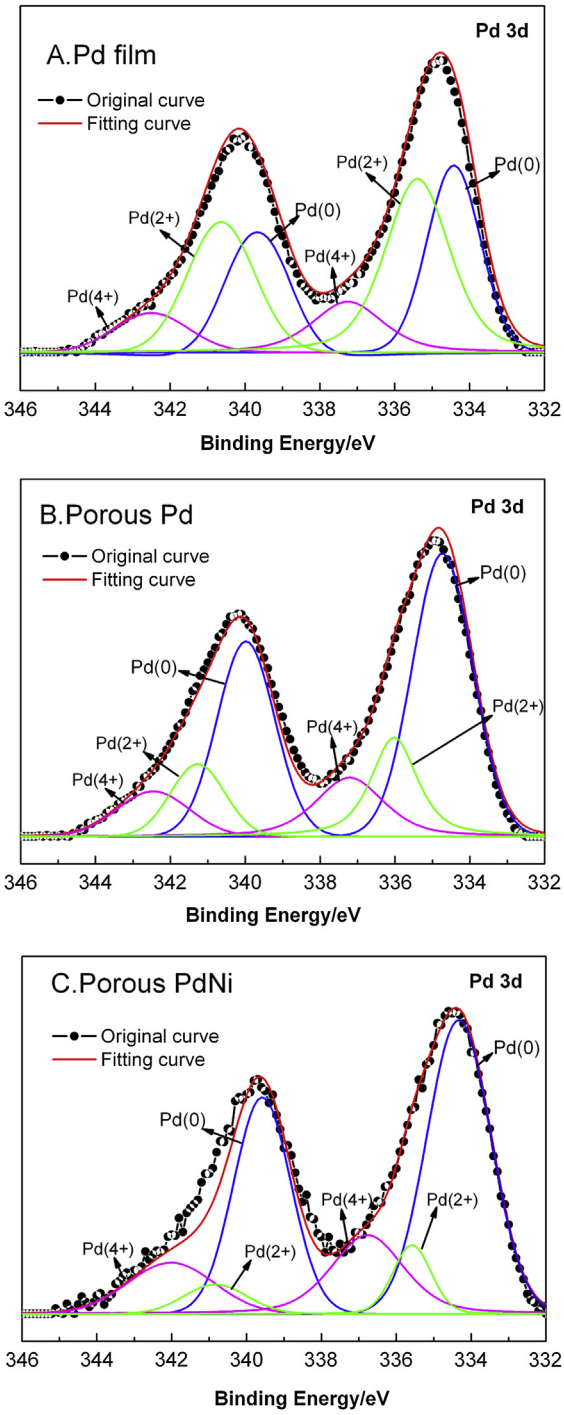

Fig. 5. Representative XPS spectra for the Pd (3d) region of the as-prepared catalysts: (A) non-porous Pd film; (B) porous Pd film; (C) porous PdNi film.

doublets, which indicates the existence of three forms of Pd. The main constituent was metallic Pd (0) at a BE of 334.42, 334.73 and 334.33 eV for non-porous Pd film, porous Pd and porous PdNi, respectively. Compared to non-porous Pd film, the positive shift of Pd (0) peaks for porous Pd can be attributed to the decrease of particle size [51,52], in accordance to the SEM images. The particle size of porous Pd and PdNi catalysts is similar, so the negative shift of Pd (0) peaks for porous PdNi is due to the slight electron transfer from Ni to Pd, consistent with the electronegativity of Pd and Ni (Pd 2.2, Ni 1.8) [53]. Therefore, the addition of Ni modifies the electronic structure and produces an electronic effect. Furthermore, the lowering of Pd 3d binding energy would influence the chemisorptions energy of adsorbate and may benefit the methanol electrooxidation [54]. The other two doublets can be ascribed to Pd (2+) and Pd (4+). The content of Pd (0) in non-porous Pd film, porous Pd and porous PdNi is 36.2%, 61.1% and 66.6%, respectively. It demonstrates clearly the decreasing contents of Pd oxides in the three kinds of catalysts. In addition, according to previous results, avoiding the formation of Pd oxides on the surface contributes to improvement of the catalytic activity and stability for Pd-based catalysts [55]. Therefore, the porous structure and Ni alloying would both help to improve the stability of the catalysts.

In order to evaluate the electronic and geometric structure of the Pd surfaces, CV experiments were conducted in 0.5 M H_2SO_4 (Fig. 6). The shape of the profile is similar to the literature [56]. The multiple peaks between −0.7 V and −0.4 V are attributed to the so-called hydrogen absorption/desorption (H_{ab}) process and hydrogen adsorption/desorption (H_{ad}) process [57]. The smaller pair of peaks at the more positive potentials is thought to be an indication of real surface area of catalysts and is missing or merged into the broad H_{ab} peaks sometimes. The significant augmentation of them indicates that the real surface area increases greatly due to the porous structure. In addition, the surface Pd oxide reduction peaks of PdNi catalyst shift negatively, which may be due to an increase in the OH adsorption strength [58]. The accurate EASA of each catalyst was calculated from the density of charge associated to the reduction of a full monolayer of Pd oxides [59,60] and the values are 3.04, 33.48 and 38.87 $m^2\ g^{-1}$, respectively. It indicates the porous structure increase the EASA by more than 10 times and the Ni alloying also increase it a little. This result corroborates the conclusion from XRD and SEM described above.

Fig. 7 shows cyclic voltammograms of methanol electrooxidation on the as-prepared catalysts in a solution of 0.5 M KOH and 0.5 M CH_3OH. The catalytic activity was evaluated as mass specific current (MSC, normalized to the mass of Pd, shown in Fig. 7A) and surface specific current (SSC, normalized to EASA, shown in Fig. 7B). In the forward scan, methanol oxidation produced an anodic peak and in the reverse scan, there was also an oxidation peak, which is attributed to methanol oxidation after the reduction of the Pd oxide and the removal of the incompletely oxidized carbonaceous species formed in the forward scan. The oxidation peak in the forward scan (j_p) is usually used to evaluate the electrocatalytic activity of the catalysts. As observed, the j_p (MSC) of the catalysts for methanol electrooxidation is 32, 154 and 238 A g^{-1} Pd, respectively, in the order of for non-porous Pd catalysts < porous Pd catalysts < porous PdNi catalysts. The current density of porous PdNi catalysts is nearly 7.4 times of non-porous Pd film and the discrepancy of the activity can be ascribed to the different EASA of the catalysts. However, compared to porous Pd catalysts, not only the activity of porous PdNi catalysts is improved by 50%, but also the current peak shifts negatively for nearly 100 mV. A little larger EASA is insufficient to account for the enhanced activity; the Ni doping effect is assumed to be more relevant. In order to evaluate the intrinsic activity of porous PdNi catalysts, the current is normalized to the real surface areas and shown in Fig. 7B. The SSC of porous PdNi catalysts is still higher than porous Pd catalysts. It indicates that the superiority of porous

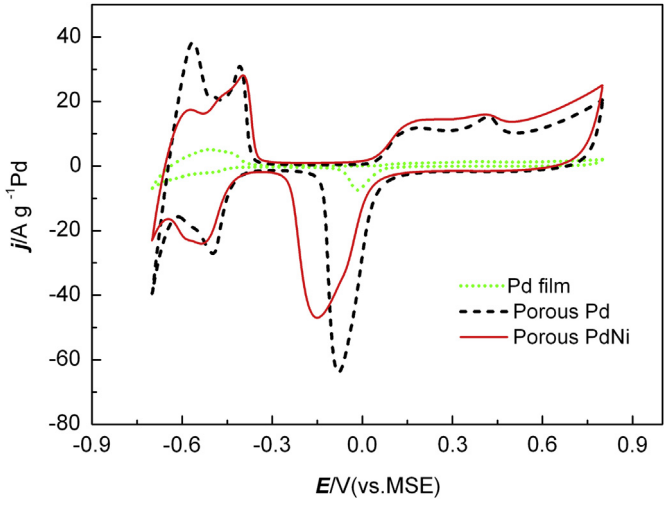

Fig. 6. Cyclic voltammograms of the catalysts in 0.5 M H_2SO_4 solution at a scan rate of 50 mV s^{-1}.

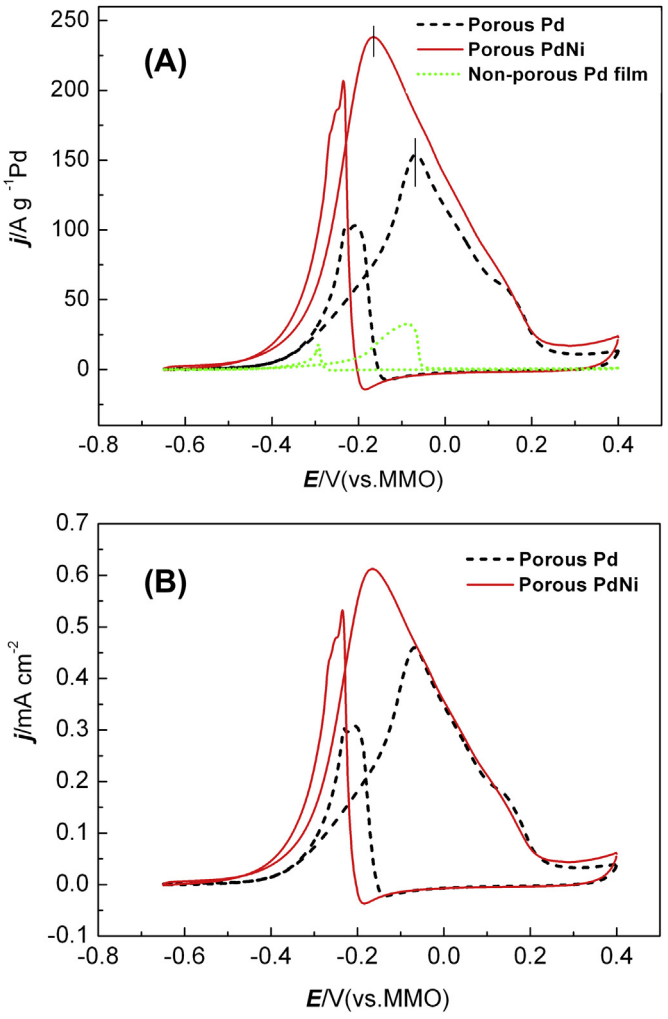

Fig. 7. Cyclic voltammograms of methanol oxidation on different catalysts in 0.5 M KOH + 0.5 M CH_3OH at a scan rate of 50 mV s^{-1}. (A) Mass specific current and (B) surface specific current.

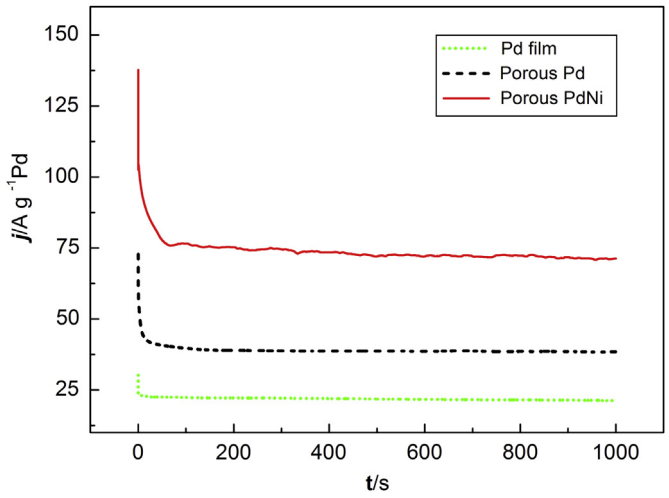

Fig. 8. Chronoamperometric curves on the catalysts in 0.5 M KOH + 0.5 M CH_3OH at −0.1 V.

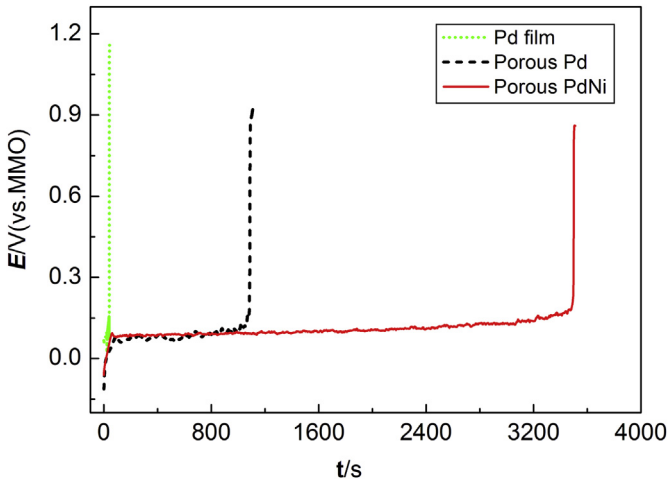

Fig. 9. Chronopotentiometric curves on the catalysts in 0.5 M KOH + 0.5 M CH_3OH with a current density of 128 mA cm^{-2}.

PdNi catalysts is not only due to the larger EASA, it also benefits from the electronic modification of Ni. It also should be mentioned the intrinsic activity of non-porous Pd catalysts isn't shown. The reasons are listed as follows: According to the recent research of F.J. Vidal-Iglesias et al. on Pd catalysts, the intrinsic activity of catalysts depends greatly on the EASA. For the same kind of catalyst, with the increasing EASA, the intrinsic activity would decrease [61]. So it's only meaningful to compare the intrinsic activity of catalysts with similar EASA. In our paper, the EASA of porous Pd and porous PdNi catalysts are similar, while the EASA of non-porous Pd catalysts is nearly 10 times smaller than that of porous catalysts. So it's only meaningful to compare the intrinsic activity of porous catalysts. According to Hammer and Nørskov's d-band center model based on DFT calculations [62,63], the Ni doping would cause the downshift of Pd's d-band center for about 0.97 eV. The lower this center lies, the lower the affinity of the metal for the adsorbate. Kibler's fundamental research [64] demonstrated that with the downshift of d-band center the Pd-based catalysts yield negative shift of peak potential for hydrogen-desorption and formic acid oxidation, indicating weaker bond of surface adsorbate. It was also reported by S. Papadimitriou et al. the downshift of d-band center would suppress the CH_3OH chemisorption (first step of methanol oxidation) and CO reaction intermediate adsorption (leading to poisoning) at the same time [65]. In our case, the Ni doping brings a suitable downshift of Pd's d-band center. Thus it decreases CO adsorption to a favorable extent without at the same time decreasing too much methanol chemisorptions. Therefore, the porous PdNi catalysts yield negative shift of peak potential and higher oxidation current for methanol oxidation. In summary, the electronic modification effect of Ni alloying can be interpreted by the d-band center model and proved by XPS and CV results.

The stability of the electrocatalysts is extremely important for their real applications in DMFCs. The long-term activity and durability of the catalysts were further assessed by CA and CP test and showed in Figs. 8 and 9. CA test was conducted on catalyst-coated GC with the potential fixed at −0.1 V. As observed, the methanol oxidation on porous PdNi possesses highest initial and limiting current densities, which indicates the best catalytic activity and stability for methanol oxidation, whereas non-porous Pd film has the lowest. CP test shows similar results, porous PdNi catalysts display a much longer steady-state behavior than the other two catalysts at a constant current as high as 128 mA cm^{-2}, which means much better stability. Likewise, porous Pd catalysts show enhanced stability than the non-porous one. The stability of the catalysts agrees quite well with the XPS results.

4. Conclusions

In summary, we synthesized porous Pd and PdNi catalysts via a facile method. The as-prepared catalysts show excellent catalytic activity and stability for methanol electrooxidation. The enhanced electrochemical performance can be ascribed to the porous structure and Ni doping which modify the electronic structure of the catalysts. In addition, it is more economic because with the doping of Ni, the using of novel metal Pd is less. And further work will aim to optimize the reaction condition such as adjusting the Ni content, choosing chelating agent and so on to perfect the structure and performance.

Acknowledgments

This work is financially supported by a grant from National Natural Science Foundation of China (No. 21003025) and Science & Technology Commission of Shanghai Municipality, China (No. 08DZ2270500).

References

[1] S. Wasmus, A. Kuver, J. Electroanal. Chem. 461 (1999) 14–31.
[2] C.K. Lin, J.C. Tsai, J. Mater. Chem. 22 (2012) 9244–9252.
[3] A.S. Arico, S. Srinivasan, V. Antonucci, Fuel Cells 1 (2001) 133–161.
[4] H.P. Liang, H.M. Zhang, J.S. Hu, Y.G. Guo, L.G. Wan, C.L. Bai, Angew. Chem. Int. Ed. 43 (2004) 1540–1543.
[5] S. Ghosh, R.K. Sahu, C.R. Raj, J. Mater. Chem. 21 (2011) 11973–11980.
[6] R. Minch, M. Es-Souni, J. Mater. Chem. 21 (2011) 4182–4188.
[7] G. Hu, F. Nitze, T. Sharifi, H.R. Barzegar, T. Wagberg, J. Mater. Chem. 22 (2012) 8541–8548.
[8] R. Liu, S. Li, X. Yu, G. Zhang, S. Zhang, J. Yao, L. Zhi, J. Mater. Chem. 22 (2012) 3319–3322.
[9] W. Wei, W. Chen, J. Power Sources 204 (2012) 85–88.
[10] E. Verlato, S. Cattarin, N. Comisso, P. Guerriero, M. Musiani, L. Vazquez-Gomez, Electrochem. Commun. 12 (2010) 1120–1123.
[11] J. Sun, Y. Wang, C. Zhang, T. Kou, Z. Zhang, Electrochem. Commun. 21 (2012) 42–45.
[12] Z.J. Mellinger, T.G. Kelly, J.G. Chen, ACS Catal. 2 (2012) 751–758.
[13] Y. Zhang, G. Chang, S. Liu, J. Tian, L. Wang, W. Lu, X. Qin, X. Sun, Catal. Sci. Technol. 1 (2011) 1636–1640.
[14] R. Kannan, K. Karunakaran, S. Vasanthkumar, Appl. Nanosci. 2 (2012) 149–155.
[15] Y. Wang, X. Wang, C.M. Li, Appl. Catal. B: Environ. 99 (2010) 229–234.
[16] R. Awasthi, R.N. Singh, Int. J. Hydrogen Energy 37 (2012) 2103–2110.
[17] Z. Yin, W. Zhou, Y. Gao, D. Ma, C.J. Kiely, X. Bao, Chem. Eur. J. 18 (2012) 4887–4893.

[18] C. Xu, A. Liu, H. Qiu, Y. Liu, Electrochem. Commun. 13 (2011) 766–769.
[19] Z. Liu, X. Zhang, L. Hong, Electrochem. Commun. 11 (2009) 925–928.
[20] Y. Zhao, X. Yang, J. Tian, F. Wang, L. Zhan, Int. J. Hydrogen Energy 35 (2010) 3249–3257.
[21] L. Chen, H. Guo, T. Fujita, A. Hirata, W. Zhang, A. Inoue, M. Chen, Adv. Funct. Mater. 21 (2011) 4364–4370.
[22] Z. Qi, H. Geng, X. Wang, C. Zhao, H. Ji, C. Zhang, J. Xu, Z. Zhang, J. Power Sources 196 (2011) 5823–5828.
[23] R.N. Singh, A. Singh, Anindita, Int. J. Hydrogen Energy 34 (2009) 2052–2057.
[24] Z. Yin, H. Zheng, D. Ma, X. Bao, J. Phys. Chem. C 113 (2009) 1001–1005.
[25] C. Zhu, S. Guo, S. Dong, J. Mater. Chem. 22 (2012) 14851–14855.
[26] C. Zhu, S. Guo, S. Dong, Adv. Mater. 24 (2012) 2326–2331.
[27] Y.Y. Chu, Z.B. Wang, Z.Z. Jiang, D.M. Gu, G.P. Yin, J. Power Sources 203 (2012) 17–25.
[28] X. Huang, S. Tang, X. Mu, Y. Dai, G. Chen, Z. Zhou, F. Ruan, Z. Yang, N. Zheng, Nat. Nanotechnol. 6 (2011) 28–32.
[29] F. Liu, Q. Yan, W.J. Zhou, X.S. Zhao, J.Y. Lee, Chem. Mater. 18 (2006) 4328–4335.
[30] F. Li, J. He, W.L. Zhou, J.B. Wiley, J. Am. Chem. Soc. 125 (2003) 16166–16167.
[31] Y. Yamauchi, A. Takai, M. Komatsu, M. Sawada, T. Ohsuna, K. Kuroda, Chem. Mater. 20 (2008) 1004–1011.
[32] G.S. Attard, S.A.A. Leclerc, S. Maniguet, A.E. Russell, I. Nandhakumar, B.R. Gollas, P.N. Bartlett, Micropor. Mesopor. Mater. 44–45 (2001) 159–163.
[33] G.S. Attard, S.A.A. Leclerc, S. Maniguet, A.E. Russell, I. Nandhakumar, P.N. Bartlett, Chem. Mater. 13 (2001) 1444–1446.
[34] P.N. Bartlett, J. Marwan, Chem. Mater. 15 (2003) 2962–2968.
[35] I.J. Brown, S. Sotiropoulos, Elctrochim. Acta 46 (2001) 2711–2720.
[36] P.J. Blood, I.J. Brown, S. Sotiropoulos, J. Appl. Electrochem. 34 (2004) 1–7.
[37] C. Xu, Y. Li, F. Tian, Y. Ding, ChemPhysChem 11 (2010) 3320–3328.
[38] H. Ji, J. Frenzel, Z. Qi, X. Wang, C. Zhao, Z. Zhang, G. Eggeler, CrystEngComm 12 (2010) 4059–4062.
[39] H.C. Shin, M. Liu, Chem. Mater. 16 (2004) 5460–5464.
[40] Y. Li, W.Z. Jia, Y.Y. Song, X.H. Xia, Chem. Mater. 19 (2007) 5758–5764.
[41] A. Ott, L.A. Jones, S.K. Bhargava, Electrochem. Commun. 13 (2011) 1248–1251.
[42] B.J. Plowman, A.P. O'Mullane, P.R. Selvakannan, S.K. Bhargava, Chem. Commun. 46 (2010) 9182–9184.
[43] S. Cherevko, C.H. Chung, Electrochem. Commun. 13 (2011) 16–19.
[44] S. Cherevko, X. Xing, C.H. Chung, Electrochem. Commun. 12 (2010) 467–470.
[45] J. Liu, L. Cao, W. Huang, Z. Li, ACS Appl. Mater. Interfaces 3 (2011) 3552–3558.
[46] S. Cherevko, N. Kulyk, C.H. Chung, Nanoscale 4 (2012) 103–105.
[47] G.M. Yang, X. Chen, J. Li, Z. Guo, J.H. Liu, X.J. Huang, Electrochim. Acta 56 (2011) 6771–6778.
[48] C. Du, M. Chen, W. Wang, G. Yin, P. Shi, Electrochem. Commun. 12 (2010) 843–846.
[49] G. Zhang, Y. Wang, X. Wang, Y. Chen, Y. Zhou, Y. Tang, L. Lu, J. Bao, T. Lu, Appl. Catal. B: Environ. 102 (2011) 614–619.
[50] Y. Suo, L. Zhuang, J. Lu, Angew. Chem. Int. Ed. 46 (2007) 2862–2864.
[51] W.P. Zhou, A. Lewara, R. Larsen, R.I. Masel, P.S. Bagus, A. Wieckowski, J. Phys. Chem. B 110 (2006) 13393–13398.
[52] M. Mazurkiewicz, A. Malolepszy, A. Mikolajczuk, L. Stobinski, A. Borodzinski, B. Lesiak, J. Zemek, P. Jiricek, Phys. Status Solidi B 248 (2011) 2516–2519.
[53] U.B. Demirci, J. Power Sources 173 (2007) 11–18.
[54] Z. Zhang, J. Ge, L. Ma, J. Liao, T. Lu, W. Xing, Fuel Cells 9 (2009) 114–120.
[55] K. Lee, O. Savadogo, A. Ishihara, S. Mitsushima, N. Kamiya, K. Ota, J. Electrochem. Soc. 153 (2006) A20–A24.
[56] J.Y. Wang, Y.Y. Kang, H. Yang, W.B. Cai, J. Phys. Chem. C 113 (2009) 8366–8372.
[57] C. Gabrielli, P.P. Grand, A. Lasia, H. Perrot, J. Electrochem. Soc. 151 (2004) A1937–A1942.
[58] W. Zhou, J.Y. Lee, J. Phys. Chem. C 112 (2008) 3789–3793.
[59] D. Morales-Acosta, J. Ledesma-Garcia, L. Godinez, H.G. Rodríguez, L. Álvarez-Contreras, L.G. Arriaga, J. Power Sources 195 (2010) 461–465.
[60] W. Pan, X. Zhang, H. Ma, J. Zhang, J. Phys. Chem. C 112 (2008) 2456–2461.
[61] F.J. Vidal-Iglesias, R.M. Aran-Ais, J. Solla-Gullon, E. Garnier, E. Herrero, A. Aldaz, J.M. Feliu, Phys. Chem. Chem. Phys. 14 (2012) 10258–10265.
[62] B. Hammer, J.K. Nørskov, Adv. Catal. 45 (2000) 71–129.
[63] J. Greeley, J.K. Nørskov, M. Maurikakis, Annu. Rev. Phys. Chem. 53 (2002) 319–348.
[64] L.A. Kibler, A.M. El-Aziz, R. Hoyer, D.M. Kolb, Angew. Chem. Int. Ed. 44 (2005) 2080–2084.
[65] S. Papadimitriou, S. Armyanov, E. Valova, A. Hubin, O. Steenhaut, E. Pavlidou, G. Kokkinidis, S. Sotiropoulos, J. Phys. Chem. C 114 (2010) 5217–5223.